

DECAY OF MULTIPLE SCALE TURBULENCE

Paolo D'Addio

Dipartimento di Ingegneria Meccanica e Aerospaziale
Università La Sapienza
Via Eudossiana 16, I-00184, Roma
paolo.daddio@uniroma1.it

Paolo Orlandi

Dipartimento di Ingegneria Meccanica e Aerospaziale
Università La Sapienza
Via Eudossiana 16, I-00184, Roma
orlandidma@dma.ing.uniroma1.it

Abstract

The decay of isotropic turbulence generated by grids was widely studied in the past, and the influence of the shape of the grid is still not fully understood. In the present work the effect of multiscale grids have been analyzed with the aim to investigate the behavior of fluid structures. A good agreement has been found with the wind tunnel experiment of *Veeravalli & Warhaft (1989)* and, despite the different Reynolds number, all the phenomena are well reproduced by DNS. The turbulence mixing layer is highly intermittent, suggesting the displacement of flow structures between the two homogeneous layers. The flow generated by the grid with the higher mesh ratio is dominated by one scale, while the flow relative to the grid with the smaller mesh ratio is controlled by two scales. The presence of a lengthscale gradient gives rise to the stress $\langle uv \rangle$. Flow visualizations of the vorticity field show that the square structures immediately behind the grid become circular before rolling-up, and that these structures survive longer for multiscale grids. The longitudinal, transverse and cross spectra show a persisting anisotropy for multiscale grids, permitting to the flow to survive longer with respect to singlescale grids. Therefore a flow with a high R_λ can be generated.

1 Introduction

A large number of studies of the turbulence generated by grids have been carried out in the past, both through wind-tunnel experiments (starting from *von Karman (1937)* and *Taylor (1935)*), and numerical simulation (*Djenidi (2004)* and *Ertunc et al. (2010)*). The flow, in a laboratory, is generated by inserting a grid in the wind tunnel. The flow is not isotropic in the region behind the grid, and becomes isotropic downstream, within a distance function of M . The flow reaches a statistical stationary steady state, with the turbulent kinetic energy q varying in the downstream direction. *Batchelor & Townsend ((1948a),(1948b))* observed that the turbulent kinetic energy was decaying with a power law x^{-m} , with $m = 1$ in the initial and $m = 5/2$ in the final period. The dependence of m on the shape of the grid has not been fully understood, however it is reasonable to presume that

the value of m is related to the vortical structures generated by the grid, and it is important to establish how far downstream the effects of the initial conditions last. *Veeravalli & Warhaft (1989)* (in the following referred to as *V&W*) investigated the flow generated by multiscale grids in wind tunnels, and *Tordella & Iovieno (2006)* analysed the effects of a gradient of integral scale into the initial conditions. In the past, simulations of isotropic decaying turbulence starting with velocity components with random phases and energy spectra peaked at different wave number were performed (*Orlandi & Antonia (2004)* among others). The initial conditions in these DNS, having random phases, differ from those in the real experiments and then the effects of the vortical structures can not be studied. The simulations should mimic, as much as possible, the conditions obtained in wind tunnels by inserting grids. Regular square grids are often used, therefore *Djenidi (2006)* and *Ertunc et al.(2010)* could use the lattice Boltzmann method to reproduce the flow past biplane grids. *Djenidi (2006)* was not interested to analyse the effects of the grid solidity, which on the other hand was investigated by *Ertunc et al.(2010)*.

The numerical method here used consists on a second order finite differences scheme with staggered velocities as described in *Orlandi (2000)*. The solid grid is reproduced by the version of the immersed boundary technique (IBM) described by *Orlandi & Leonardi (2006)*. As in the wind tunnels at the inlet the flow is uniform and the experimental disturbances are reproduced by a random velocity field of small amplitude, which is necessary to produce the turbulence. The large scales and hence the energy containing eddies are generated by the solid grid.

2 Results

2.1 Simulation details

The shape of the grid dictates the velocity distribution at its exit and it has been checked that if the grid is located at $L_G = 2$ the velocity profiles at the exit do not change. The number of points is 1153 in the x direction and 192 in the y and z directions. The dimensions of the domain are $L_1 = 18\pi$ and $L_2 = L_3 = 2\pi$. The boundary conditions are

periodic in the y and z directions and radiative at the outlet in x . The grids used for the simulation are shown in Fig.1 and the geometric parameters are listed in Tab.1.

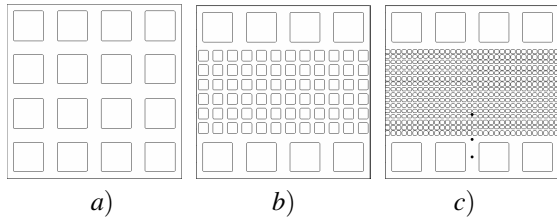


Figure 1. Geometry of the grids a) G_{4-4} , b) G_{12-4} , c) G_{32-4} . Solid points indicate the position of the wires (see Sec.2.3)

The mesh of the grid is defined as $M = \frac{2\pi}{N_a}$, where N_a indicates the number of voids in a row, it is equal to $M = \frac{2\pi}{4}$ for the single scale grid G_{4-4} . For the multiscale grids N_a assumes two values. r is the solidity of the grid, defined as the ratio between the solid volume and the total volume: $r = \frac{V_{solid}}{V_{tot}}$. The flow has been analyzed at two Reynolds number $Re = \frac{U_1 L_2}{\nu} = 1500$ and $Re = 3000$. The inlet disturbances at $t = 0$ are convected downstream and, at a certain time, reach the outlet section. Only after this time the fields are saved to calculate the statistics. Thirty fields are sufficient to eliminate the streamwise oscillations found by averaging one field in the homogeneous direction.

2.2 Energy decay

The large differences in the meshes of the grids allow to have informations on the effect of the initial conditions on the decay of isotropic turbulence. The decay law is $q = a(\frac{x}{M_L} - X_0)^{-m}$. The values for m have been evaluated by a best fit of the q profiles for $\frac{x}{M_L} > 10$ and are listed in Tab.1.

The trend of $\langle q \rangle$ (Fig.2a) in the anisotropic region ($\frac{x}{M_L} < 5$) indicates that the smaller mesh of the grid influences the distance where the energy starts to decay. The decay is anticipated by reducing the size of the smaller mesh (G_{32-4}). On the other hand, the presence of two very different meshes let the flow survive longer, ensuring a smaller m . So, despite the anticipated decay for the multiscale grids, at the end of the domain, the turbulent energy is higher with respect to the singlescale grid. Comparing the multiscale grids G_{12-4} and G_{32-4} it is evident that the energy is better conserved by increasing the mesh ratio. The two multiscale grids are fitted with a good approximation by the line $(x/M_L)^{-1.1}$. On the other hand the singlescale grid is fitted by $(x/M_L)^{-2.4}$, proving that different scales allow the flow to survive longer. The initial Reynolds number for the singlescale grid leads to a fast decay, typical of the final period of decay (Batchelor & Townsend (1948b)), while the combination of different meshes in the same grid allows a slower decay with $m \approx 1$, typical of the initial period of decay (Batchelor & Townsend (1948a)). The Reynolds number based on the Taylor microscale, calculated as $Re_\lambda = \frac{\lambda_g \sqrt{u_i^2}}{\nu}$, and plotted in Fig.2b, confirms the last statement. While Re_λ for the single-scale grid decreases, the multiscale grids allow to generate a flow with a value of Re_λ that remains constant, and even increases.

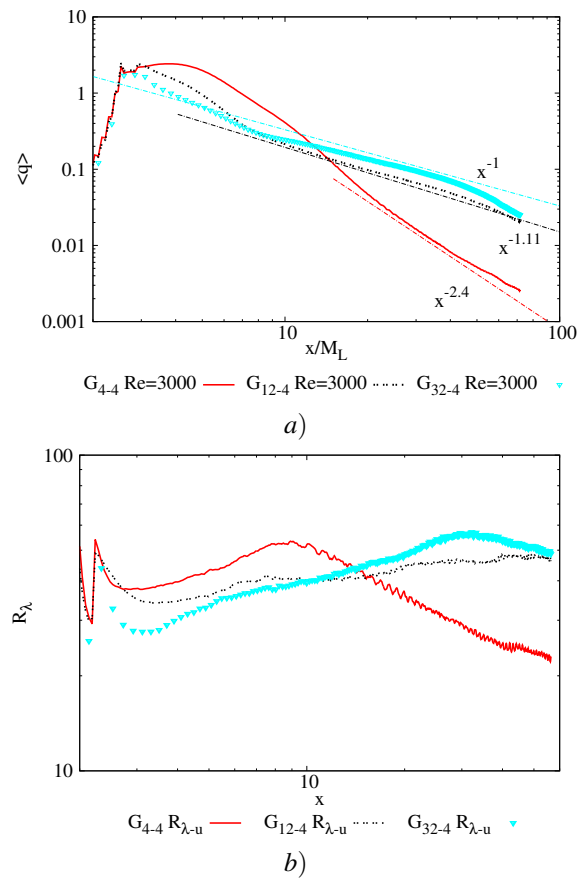


Figure 2. a) Turbulent kinetic energy as function of the non-dimensional distance for G_{4-4} , G_{12-4} and G_{32-4} at $Re = 3000$ with the relative slope. b) Profiles of Re_λ versus x at $Re = 3000$.

2.3 Intermittency

One of the aims of the present study is to corroborate the existence of intermittency in presence of a lengthscale gradient, observed in the wind tunnel experiments by V&W. The intermittency was detected by analyzing the statistics at the interface between the two homogeneous flows, dominated by two different scales. For this reason three wires have been located respectively in the high-turbulence region, in the mixing layer and in the low-turbulence region. In Tab.1 are listed the set-up in the present work and in the experiment by V&W, and in Tab. 2 are reported the values of skewness and flatness for the grid G_{32-4} at $Re = 3000$.

The statistics of the two velocity components reveal that the mixing layer is more intermittent than the two homogeneous layers. The flatness suggests that the difference between the three layers is more evident for the v -component. The high intermittency of the mixing layer was related by V&W to the migration of the vortical structures from one homogeneous layer to the other. The positive values of the skewness in this region, demonstrate that the structures move from the large towards the small scales.

2.4 Variance profiles

Fig.3 and Fig.4 show normalized $\langle u^2 \rangle$ and $\langle v^2 \rangle$ profiles taken at different downstream location, for the multiscale grids. In the figures are also reported the data of V&W for the 3 : 1 perforated plate and 8.9 : 1 bar grid. To verify the flow self-similarity, the profiles have been normalized

August 28 - 30, 2013 Poitiers, France

Table 1. Flow parameters for the grids. Re_{M_S} is the Reynolds number evaluated with the small mesh as reference length. (*: values relative to $Re = 3000$. **: evaluated as the average between the exponent for the large-scale and that of the small-scale region).

	$M_S : M_L$	r	Re_{M_S}	m
G_{4-4}	1 : 1	0.57	750*	2.39*
G_{12-4}	1 : 3	0.57	250*	1.11*
G_{32-4}	1 : 8	0.57	125*	1.09*
$V\&W_{bars}$	1 : 3.3	0.32	3505	1.41**
$V\&W_{bars}$	1 : 8.9	0.29	1744	—
$V\&W_{plate}$	1 : 3	0.31	4060	1.34**

Table 2. Values of skewness and flatness of the velocity fluctuations averaged in time for the grid G_{32-4} at $Re = 3000$. Wires are located at $x = 7.54M_L$, $z = 1.98M_L$, at three different position along y : $y_{small} = 0.48M_L$, $y_{mixing} = 0.94M_L$, $y_{large} = 1.60M_L$ as shown in Fig.1.

	$\frac{\langle u^3 \rangle}{\langle u^2 \rangle^{3/2}}$	$\frac{\langle u^4 \rangle}{\langle u^2 \rangle^2}$	$\frac{\langle v^3 \rangle}{\langle v^2 \rangle^{3/2}}$	$\frac{\langle v^4 \rangle}{\langle v^2 \rangle^2}$
y_{small}	-0.258	3.131	0.229	2.819
y_{mix}	0.682	3.449	0.538	3.849
y_{large}	0.267	2.977	-0.088	2.456

and scaled by mapping the small-scale end to zero and the large-scale end to one. The y -axis is normalized through $\bar{y}(y) = \frac{1}{2}(y_{u=0.75} + y_{u=0.25})$ and $\delta(y) = y_{u=0.75} - y_{u=0.25}$ (where $y_{u=0.75}$ is the point where $\langle u^2 \rangle = 0.75$, and similarly $y_{u=0.25}$ is the point where $\langle u^2 \rangle = 0.25$) leading to $\xi = \frac{y - \bar{y}(y)}{\delta(y)}$. For the variance $U_C^2 = \frac{1}{2}(U_{max}^2 + U_{min}^2)$ and $U_S^2 = U_{max}^2 - U_{min}^2$ have been used to obtain $f(\xi) = \frac{\langle u^2 \rangle - U_C^2}{U_S^2}$. The same normalization has been used for $\langle v^2 \rangle$.

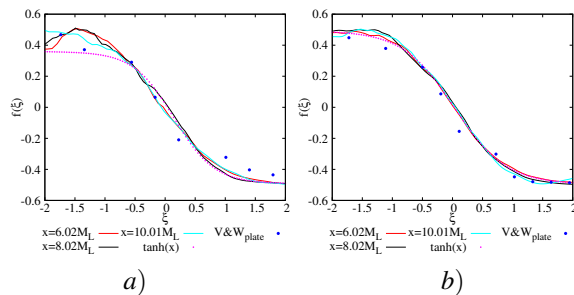


Figure 3. Normalized variance profiles for G_{12-4} at different distance x at $Re = 3000$. a) $\langle u^2 \rangle$ and b) $\langle v^2 \rangle$. Data relative to the experiment of V&W for the 3 : 1 perforated-plate at $x = 27.2M_L$ are also reported.

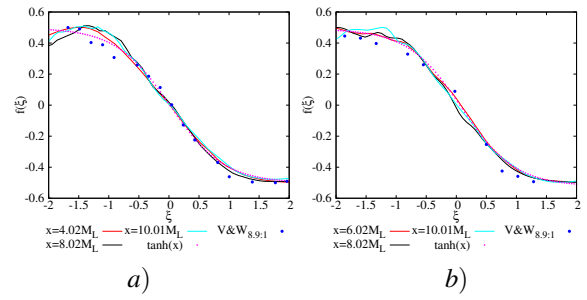


Figure 4. Normalized variance profiles for G_{32-4} at different distance x at $Re = 3000$. a) $\langle u^2 \rangle$ and b) $\langle v^2 \rangle$. Data relative to the experiment of V&W for the 8.9 : 1 bar grid at $x = 28.9M_L$ are also reported.

The collapse of the profiles is remarkably good for G_{32-4} , for both $\langle u^2 \rangle$ and $\langle v^2 \rangle$, indicating that the flow is self-similar. The profiles are well fitted by the function $y = \tanh(x)$, with small departures from this curve for $\langle v^2 \rangle$. Larger departures are instead present for $\langle u^2 \rangle$, especially in the large-scale region. The results agree with those by V&W who deduced from this behavior that the large scales dominate the flow. In addition they reported that for the 3 : 1 grids large deviations from the fitted curve are present, especially in the high-turbulence side of the flow. Our results for G_{12-4} confirm their observations therefore, differently from the 8.9 : 1 grid, it can be asserted that two scales dominate the flow of G_{12-4} .

For a better understanding of the downstream evolution, the profiles of $\langle u^2 \rangle$ versus y at different distances from the grid are presented (Fig.5). Close to the grid ($x = 2.03M_L$) the geometry dictates the shape of the profile. Departing from the grid the flow begins to homogenize. In correspondence of the smaller meshes, at the distance $x = 4.02M_L$, the energy for the grid G_{32-4} is smaller than that of the G_{12-4} and G_{4-4} . This happens because the difference between the scales does not allow the eddies to interact, and the smaller scales sharply decay. After this rapid energy decay of the small scales, the transport from the large to the smaller scales allows to the flow at the center to maintain approximately the same value of $\langle u^2 \rangle$ reached at $x = 4.02M_L$. This phenomenon for G_{12-4} is barely visible at $x = 6.02M_L$, and at $x = 8.02M_L$. At $x = 31.94M_L$, where a good condition of homogenization is reached, the value of $\langle u^2 \rangle$ for G_{32-4} is about 0.01, higher than $\langle u^2 \rangle$ for G_{12-4} , that are much higher than $\langle u^2 \rangle$ for G_{4-4} . Thus the transfer of energy from the large towards the small-scale leads to a weaker decay. Only at the high mesh ratio a dependence from the Reynolds number appears. In fact the grids G_{4-4} and G_{12-4} do not present substantial differences in the profiles at $Re = 1500$ and $Re = 3000$. Instead in the profiles of G_{32-4} differences between $Re = 1500$ and $Re = 3000$ are evident at $x = 8.02M_L$, especially in the central region, dominated by the small scales. These differences disappear once the flow is homogenized.

2.5 Vorticity field visualization

The visualizations of the vorticity field help to explain the reduction of the energy decay for multiscale grids. Flow structures can be easily detected by $|\omega|$ visualizations in Fig.6.

High values of vorticity magnitude for the grid G_{4-4} in correspondence of the edge of the holes ($x = 1.27M_L$) are

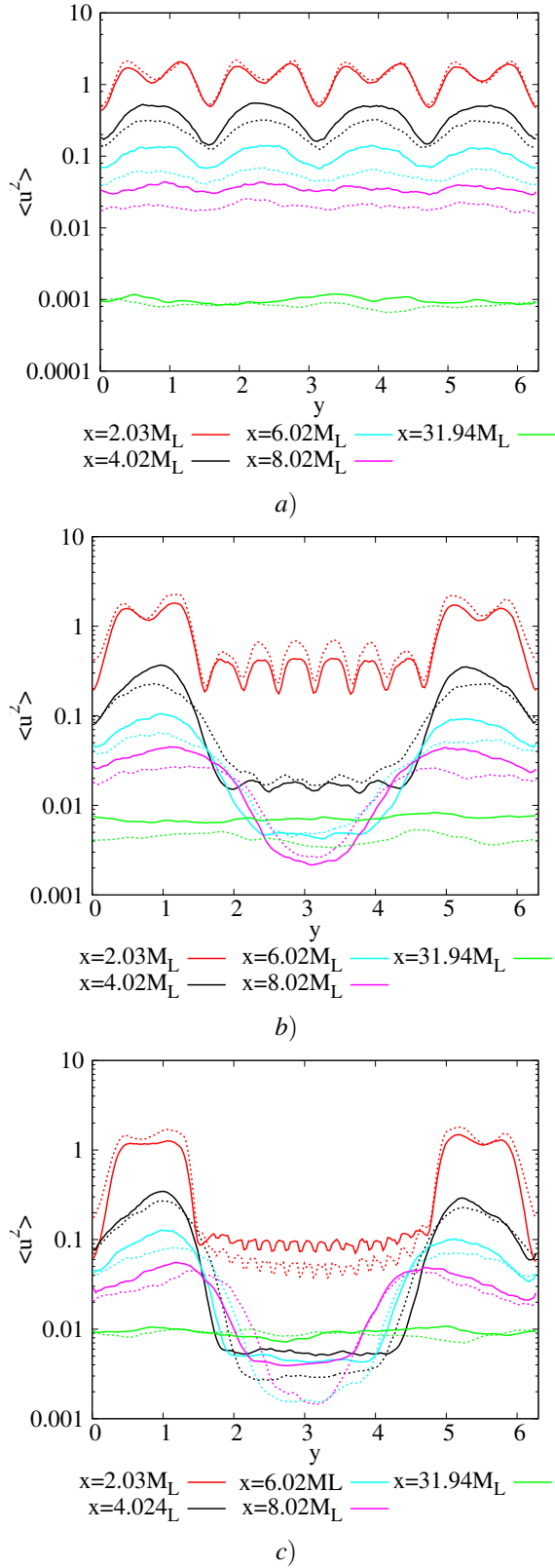


Figure 5. Profiles of variance $\langle u^2 \rangle$ at different distances for a) G_{4-4} , b) G_{12-4} and c) G_{32-4} . Solid lines, $Re = 3000$. Dashed lines, $Re = 1500$.

concentrated in a thin region of square shape. These squares tend to roll-up to form tube-like structures. This passage occurs through a transformation of the layers of square shape in circular layers at $x = 1.59M_L$.

The 3D surface contours of the three vorticity com-

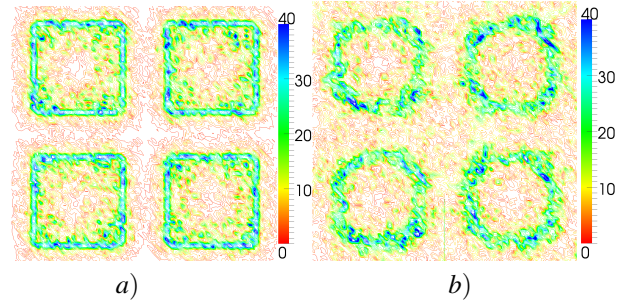


Figure 6. Contour of $|\vec{\omega}|$ for a quarter of the grid G_{4-4} with $Re = 3000$ at a) $x = 1.27M_L$, b) $x = 1.59M_L$.

ponents in Fig.7 show the formation of sheet-like structures in correspondence of the edges, made of $|\vec{\omega}_2|$ and $|\vec{\omega}_3|$ respectively. The vortex-stretching breaks down the sheets and forms tube-like structures characterized also by the presence of $|\vec{\omega}_1|$.

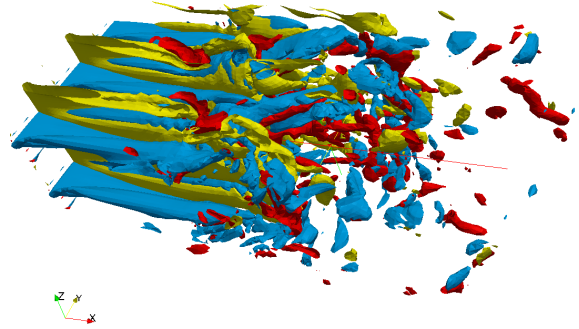


Figure 7. Surface contour of $|\vec{\omega}_1|$, $|\vec{\omega}_2|$ and $|\vec{\omega}_3|$ respectively in red, blue and yellow, for a section of the grid G_{4-4} with $Re = 3000$. $|\vec{\omega}_1| = 20$.

The analysis of the structures generated by the multi-scale grid G_{32-4} is in Fig.8. The contour plot at $x = 1.59M_L$ compared with that relative to the grid G_{4-4} enlights that the sheet-like structures generated by the larger meshes, maintain the squared-form, differently from the G_{4-4} where the instability has already produced circles. This implies that the large eddies hold for a long distance. The large difference in the dimension of the meshes does not allow the bigger structures to interact with the smaller ones located at the center, but the interactions are restricted to the region characterized by a similar lengthscale. The same argument is valid for the smaller scales that, as expected, decay faster. Fig.8 at $x = 6.37M_L$ depict isotropy for the smaller scales and a coherence for the large scale that, at the same time penetrate towards the center.

2.6 Spectral analysis

To have an idea of the isotropy at small scales the longitudinal and the transverse one-dimensional spectra should be compared with those by DNS of forced isotropic turbulence (Jimenez *et al.* (1993)). The comparison necessitates the Kolmogorov normalization. The rate of dissipation ϵ has been calculated by the one-dimensional spectra ($\epsilon = 15\nu \int \kappa_i^2 E_{ii} d\kappa_i$). The Kolmogorov scale $\eta = (\epsilon/\nu^3)^{1/4}$, gives the non-dimensional wave number $\kappa_i^* =$

August 28 - 30, 2013 Poitiers, France

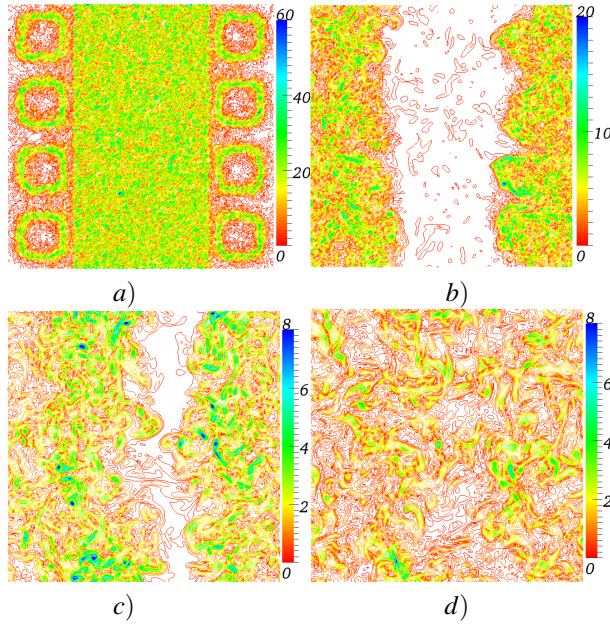


Figure 8. Contour of $|\omega|$ for the whole field of the grid G_{32-4} with $Re = 3000$ at a) $x = 1.59M_L$, b) $x = 6.37M_L$, c) $x = 14M_L$, d) $x = 19.1M_L$

$\kappa\eta$, and the one-dimensional dimensionless spectra are $E_{ii}^* = E_{ii} (\varepsilon/v^5)^{-1/4}$.

The sharp energy peaks in the spectra at $x = 2.03M_L$ (Fig.9a) indicate the strong influence of the grid. The energy, inserted at the wave number proportional to the mesh of the grid, has not been transferred into the whole range of wave numbers. In fact a true exponential range is not formed. Further downstream, at $x = 16M_L$, Fig.9b indicates a collapse of all the spectra in the exponential range with those obtained by the *Jimenez et al. (1993)*. This figure in addition proves that the present DNS is fully resolved.

The spectra allow also to get information about the isotropy. Approaching isotropy the co-spectra $E_{13}^*(k_3^*)$ and $E_{21}^*(k_2^*)$ tend to overlap. Fig.10a shows that at $x = 31.94M_L$ the isotropy is not achieved for the multiscale grid G_{32-4} . The anisotropy can be appreciated also by the plots of the Reynolds stresses $\langle uv \rangle$, $\langle uw \rangle$ (Fig.10b), where it is evident that the stress $\langle uv \rangle$ for the G_{32-4} tends to zero smoothly, and also at $x = 31.94M_L$ is not identically zero. The plots relative to the Reynolds stresses agree once again with the results of *V&W*. As they noted, the presence of a mean velocity gradient gives rise to a turbulence mixing-layer, and $\langle u^2 \rangle$ can not be equal to $\langle v^2 \rangle$. Then $\langle uv \rangle$ can not be zero within the mixing layer.

3 Conclusions

In the present work the decay of multiple scale generated turbulence has been studied through DNS to have a better understanding of the effects of the shape of the grid, assumed similar to those used in the experiments by *Veeravalli & Warhaft (1989)*. The value of the decay exponent of the single scale grid ($m \approx 5/2$) suggests that the flow, at $Re = 3000$, is in the final period of decay where the spectrum is dominated by the exponential range. The comparison between simulations with single and multiple scale grids demonstrated that the latter lead to a reduction of the decay exponent, approximately $m \approx 1$. The decrease

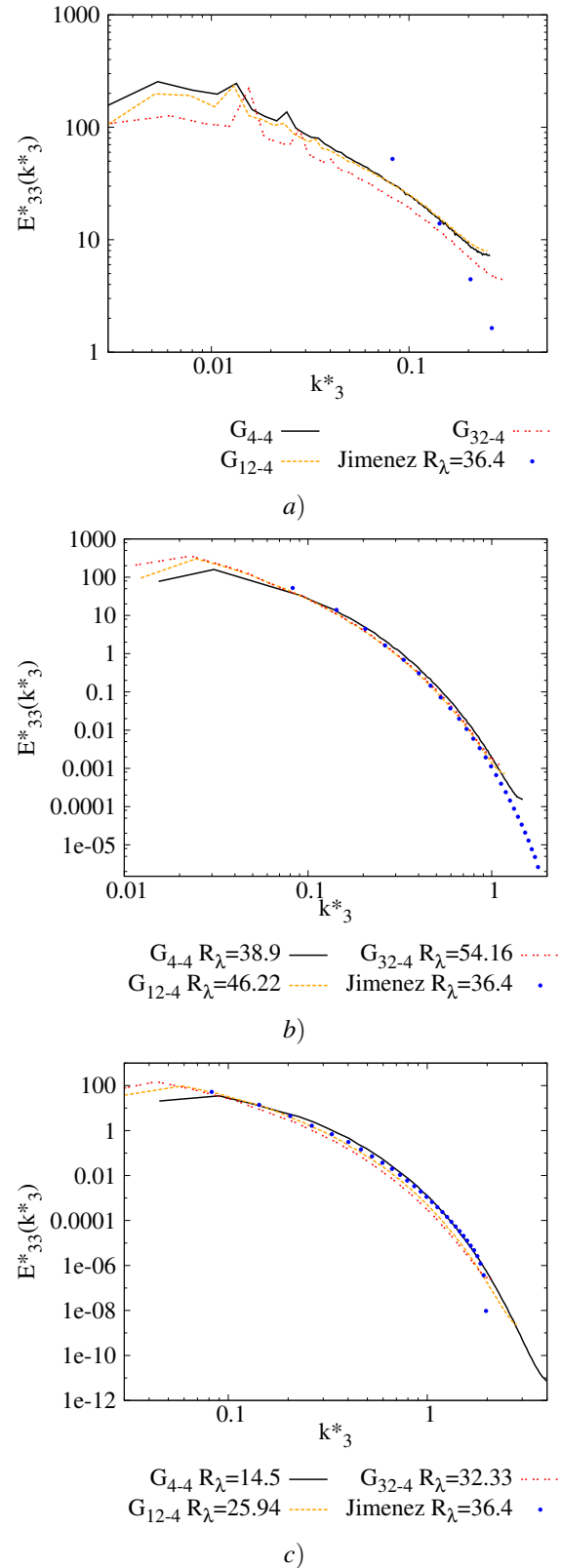


Figure 9. Profiles of dimensionless one-dimensional longitudinal spectra in Kolmogorov variable ($E_{33}^*(k_3^*)$) for G_{4-4} , G_{12-4} and G_{32-4} at $Re = 3000$. a) $x = 2.03M_L$, b) $x = 16M_L$ and c) $x = 31.94M_L$.

is accompanied by a higher Re_λ that, differently from the single-scale grid, remains constant and even increases, similar to the experiments with fractal grids (*Seoud & Vassilicos (2007)*). The aim of the present work has been focused on

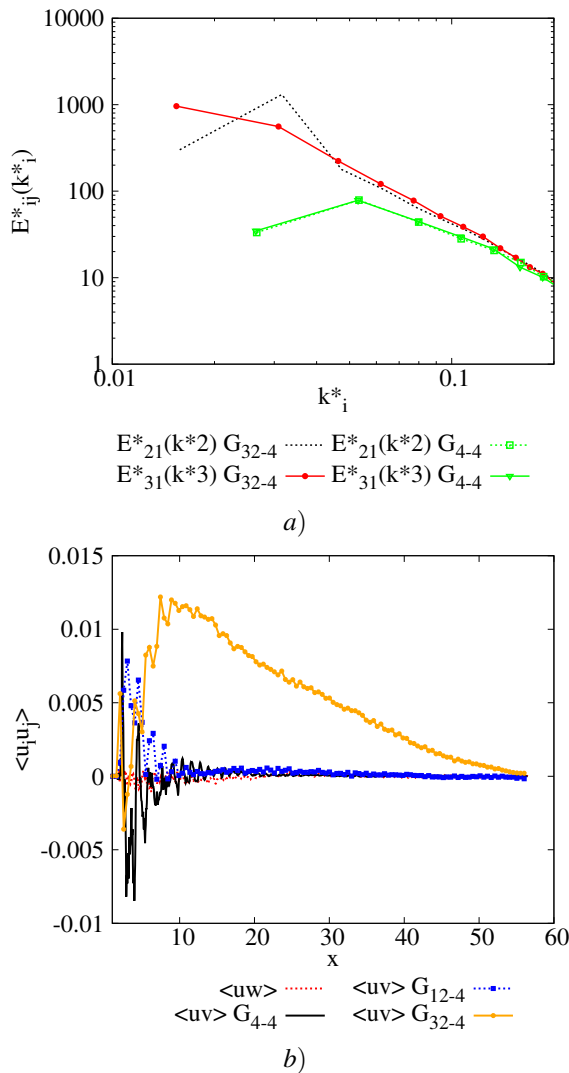


Figure 10. a) Kolmogorov spectra $E_{31}^*(k_3^*)$ and $E_{21}^*(k_2^*)$ for G_{4-4} and G_{32-4} . b) Mixed Reynolds stress $\langle uv \rangle$ and $\langle uw \rangle$ versus the distance x , for G_{4-4} , G_{12-4} and G_{32-4} at $Re = 3000$.

analyzing the space evolution of the structures. The statistics have shown a high intermittency in the mixing layer when the difference in the meshes is large (G_{32-4}). The small departures from a best fitting error of the rms, for the same grid G_{32-4} , have demonstrated that just one scale governs the flow. The flow visualizations of the fluid structures, show that multiscale grids let the sheet-like structures survive longer. Spectra of multiscale grids have indicated that the energy contained at smaller κ decays less than that for singlescale. This behaviour suggests that for single-scale grids, the eddies of comparable dimensions interact more efficiently, facilitating the energy cascade. This may suggest that in isotropic turbulence local interactions occur both in physical and in wave number space. The coexistence of very different scales instead causes the smaller eddies to die suddenly. The large eddies, unable to interact with the small ones, maintain their coherence longer, dif-

fusing towards the region dominated by the smaller meshes. This hypothesis can easily explain the intermittency measured at the interface between the two homogeneous layers, caused by the movement of fluid structures from the large scales region towards the small scale region. The fact that the scales generated by the small mesh die suddenly, letting the flow being dominated by the large ones only, is corroborated by the cross-stream profiles of the velocity variance. Multiscale grids generate a flow with high Re_λ and a small decay coefficient. Nevertheless, these characteristics imply that the flow remains non-homogeneous for a long distance, as shown by the rms profiles and by the spectra in the exponential range. The good collapse of the spectra in the exponential range demonstrates also the quality of the numerical method.

4 References

- Batchelor, G. K. & Townsend, A. A., 1948 *Decay of Turbulence in the Final Period*. Proc. R. Soc. Lond. A 194, pp. 527-543
- Batchelor, G. K. & Townsend, A. A., 1948 *Decay of Isotropic Turbulence in the Initial Period*. Proc. R. Soc. Lond. A 193, pp. 539-558
- Djenidi, L. 2006 Lattice-Boltzmann simulation of a grid-generated turbulence, Journal of Fluid Mech. 552, pp. 13 - 35
- Ertunc, O., Ozyilmaz, N., Lienhart, H., Durst, F. Beronov, K., 2010 Homogeneity of turbulence generated by static-grid structures, Journal of Fluid Mech. 654, pp. 473 - 500
- Jimenez, J. Wray, A. A. Saffman, P. G. & Rogallo, R. S., 1993 *The structure of intense vorticity in isotropic turbulence*. J. Fluid Mech., 255, pp 65-90, the data are available in AGARD AR-345 1998.
- Orlandi, P., 2000 *Fluid Flow Phenomena : A Numerical Toolkit*, Kluwer.
- Orlandi, P. & Antonia, R. A., 2004. *Dependence of a passive scalar in decaying isotropic turbulence on the Reynolds and Schmidt numbers using the EDQNM model*. Journal of Turbulence 5 .pp. 009 .
- Orlandi, P. & Leonardi, S., 2006. *DNS of turbulent channel flows with two- and three-dimensional roughness*. Journal of Turbulence. Vol. 7, No. 53, 1468-5248.
- Seoud, R. E. & Vassilicos, J. C., 2007 *Dissipation and decay of fractal-generated turbulence* Phys. Fluids 19, pp. 105108
- Tordella, D. & Iovieno, M., 2006. *Numerical experiments on the intermediate asymptotics of shear-free turbulent transport and diffusion*. J. Fluid Mech., 549, pp 429-441
- Veravalli, S. & Warhaft, Z., 1989. *The shearless turbulence mixing layer* J. Fluid Mech., 207, pp 191-229.
- Taylor, G.I., 1935 *Statistical theory of turbulence* Proc. R. Soc. Lond. A, Vol.151, pp.421-454.
- von Karman, T. , 1937 *The fundamentals of the statistical theory of turbulence* J. Aer. Sci., Vol.4, pp.131-138.